



Contents lists available at ScienceDirect

Nuclear Inst. and Methods in Physics Research, A

journal homepage: www.elsevier.com/locate/nima

Tensile, flexural, and light output measurements of selected organic scintillators for evaluation of their potential as structural materials

Caleb Redding^{a,*}, Alexandra Hackett^{a,1}, Mitchell Laubach^{a,2}, Rui Feng^a, Patrick Feng^b, Chuck Hurlbut^c, Peter Liaw^a, Jason P. Hayward^a^a Department of Nuclear Engineering, The University of Tennessee, Knoxville, TN, United States^b Sandia National Laboratory, Livermore, CA, United States^c Eljen Technology, Sweetwater, TX, United States

ARTICLE INFO

Keywords:

Unmanned radionuclide search
Organic scintillators
Mechanical testing
Polymer crosslinking
Organometallic complex

ABSTRACT

In order to design structures, such as unmanned vehicle structures, out of plastic scintillator, e.g., for radionuclide searches, suitable materials must either be identified or developed. In searches utilizing unmanned vehicles, the absence of an additional detector attached to the vehicle body as a payload could enable the vehicle to travel faster, carry a longer lived battery, or carry other auxiliary equipment which may be useful for search and/or response. To this end, four mechanical characteristics of selected organic scintillators manufactured by Eljen technologies, Sandia Livermore, and Lawrence Livermore National Lab have been measured. Specifically, tensile and flexural tests have been performed to ASTM specifications on organic scintillators with polyvinyl toluene (PVT), polystyrene (PS), or crosslinked versions of these bases. In addition to these mechanical tests, light output testing was performed in order to quantify whether crosslinking or adding organometallic complexes affects light output in the particular scintillator compositions we measured. We found that the tested plastic scintillators have strengths that are comparable to common structural plastics. We also show that chemically modifying the polymer base can show improvements in the mechanical properties without being overly detrimental to the scintillator light output.

Contents

1. Introduction	1
2. Materials and methods.....	2
2.1. Tensile testing	2
2.2. Flexural testing.....	2
2.3. Light output testing	3
3. Results and discussion	3
3.1. Tensile test results	3
3.2. Flexural test results.....	4
3.3. Light output testing	4
4. Conclusion	5
Acknowledgments	6
References.....	6

1. Introduction

Solid organic scintillators find common use as radiation detectors for national defense and homeland security applications due to their

low cost and reliability. Common forms include polyvinyl toluene (PVT) and polystyrene (PS). Important advances in the last decade have included successes in high Z loading in solid organic scintillators [1–3], fabrication of solid organic scintillators with good pulse shape

* Corresponding author.

E-mail address: creddin2@vols.utk.edu (C. Redding).¹ Currently at Oak Ridge National Laboratory, Oak Ridge, TN.² Currently at Canberra Industries, Oak Ridge, TN.

<https://doi.org/10.1016/j.nima.2018.10.126>

Received 31 July 2018; Accepted 16 October 2018

Available online xxxx

0168-9002/© 2018 Elsevier B.V. All rights reserved.

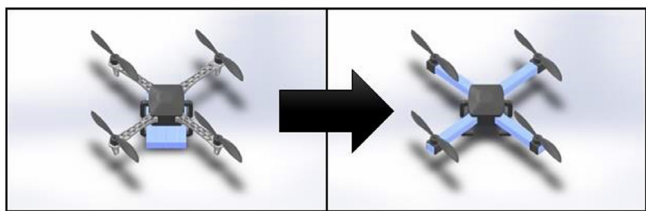


Fig. 1. Illustration of UAV structural modification to include organic scintillator (shown in blue) as part of the vehicle body instead of adding a dedicated detector to the vehicle payload. (For interpretation of the references to color in this figure legend, the reader is referred to the web version of this article.)

discrimination characteristics [4–7], and methods advances allowing for improved spectroscopy with large solid organic scintillators [8]. Mechanically robust, solid organic scintillators may be particularly useful in applications where it is desirable for the detector material to also function as a mechanical component of an apparatus which may be used for the detection of special nuclear material (SNM) or other radionuclides. An example of such an application is utilizing the detector material as part of the frame of a vehicle for unmanned SNM searches.

One focus of this study is to determine whether solid organic scintillators could be used as a structural material, for example, as an airframe for a lightweight unmanned aerial vehicle (UAV). Due to the limited payload capacity of lightweight UAVs, on-board SNM detectors should not significantly add to the weight of the UAV. One potential solution to this problem is to utilize the detector material as the primary component of the UAV airframe, as shown in Fig. 1. In this situation, the detectors are integrated as part of the UAV body and account for a significant portion of the vehicle's overall weight and mechanical integrity. An additional focus of this study is to report on the effect of polymer crosslinking on scintillator strength and light output. Since it is expected that crosslinking may improve the mechanical robustness of the scintillator, it is important to understand what, if any, trade-offs exist and to what degree they affect the detector performance. Since light yield is directly related to energy resolution, pulse shape discrimination performance, and other performance properties, it is an important property to understand as changes are made to the polymer matrix.

2. Materials and methods

A large variety of materials are potential candidates to serve the dual purpose role of vehicle frame (or other structural plastic) and radiation detector. The material selection for this study is provided in Table 1. All materials were fabricated by Eljen Technologies, with the exception of the PD-02-55.02 materials fabricated by Patrick Feng's group at Sandia National Lab Livermore. The materials selected for this study were chosen with the intent to probe existing material candidates which are either commercially available or are not yet fully commercialized but are in the late stages of development. In order to study the effect of crosslinking the polymer base, the commercially available materials were requested to be manufactured with and without crosslinking of the base. The crosslinked samples are tagged with "XL" in the label. In addition to crosslinking, two standard bases were also compared while using the same fluors as exhibited by the EJ-200 vs. EJ-200PS which have PVT and PS bases respectively. An additional variable whose effect was examined is the addition of tin-containing organometallic complexes to the PD-02-55.02 scintillator. This material is tested with and without 5% by weight of the tin organometallic complex.

2.1. Tensile testing

The tensile test samples were machined from a bulk sheet or boule of material into large type IV and/or small type V dog-bone shapes.

Table 1

Selected material types and description.

Test material	Description
EJ-200	Standard PVT polymer base and manufacturing process
EJ-200PS	Standard PS polymer base and manufacturing process
EJ-200PS-XL	PS base with crosslinked polymers
EJ-299-33	PSD plastic without crosslinking
EJ-299-33-XL	PSD plastic scintillator with crosslinked polymers
PD-02-55.02	PS-based plastic made at SNL Livermore
PD-02-55.02(Sn)	Tin-loaded, PS-based plastic made at SNL Livermore
N555V	Recent plastic commercialized by LLNL

The dimensions of these sample types are fully defined in the ASTM test standard D638 [9] which also served as the primary basis for the experimental guidelines. The measurements were performed using an MTS 810 servohydraulic load frame equipped with an MTS 647 hydraulic wedge system and controlled by the MTS Multi-Purpose Testware software. The tensile strain was recorded by the software using data generated by the MTS 634.31E–24 extensometer which was set to a gauge length of 12.5 mm. The rate of separation of the crosshead is provided in Table 2 along with other experimental parameters such as the data sampling rate, nominal cross-sectional area of the narrow section of the sample, and whether or not the nominal or measured cross-sectional area was used for calculating the stress on the sample. A small pre-load force (~18 N) was applied to all samples in order to remove slack in the system prior to recording data.

Using the strain and applied force data, stress vs. strain curves were then constructed. From this data the maximum tensile stress and the tensile modulus of each material sample were determined. The tensile stress is defined as the applied force divided by the cross-sectional area of the narrow portion of the sample. In order to find the maximum tensile stress, the stress vs. strain data was first smoothed using a centered moving average containing 21 data samples. The number of data samples in the moving average was chosen to minimize the mean square error (from adding too many data points) and to also minimize the oscillatory effect in the mean square error which is observed from adding in additional data points for inclusion in the mean calculation (a result of having too few data points). The maximum value in the stress data was then found and recorded for each sample. The tensile modulus is defined as the slope of the stress vs. strain curve. The modulus of each material sample was calculated using a minimum of 400 non-smoothed data samples taken from the Hookean (proportional) region of the stress vs. strain curves and determining the line-slope by using the least squares methodology.

2.2. Flexural testing

In a manner similar to the tensile test samples, the samples for the flexural tests were also machined from large sheets or boules of bulk material into one of two sample sizes. The choice between the two sizes was made based upon the largest available sample sizes for any particular plastic scintillator. The large samples were machined to have nominal dimensions of $127 \times 25.4 \times 25.4$ mm (length \times width \times depth) while the small samples were machined to nominal dimensions of $65 \times 12.7 \times 3.2$ mm. The testing procedures utilized for this portion of the study were derived from the ASTM standard for flexural testing, D790 [10]. The physical setup of the measurement equipment is nearly identical to the setup used for the tensile tests with two caveats: (1) the hydraulic grips are used to hold the upper and lower components of the flexural testing apparatus instead of the sample directly and (2) there is no need for use of an extensometer as the position of the loading nose is controlled directly by the system software. The flexural testing apparatus consists of a lower component that has two points of contact separated by a variable span, L . The upper component of the apparatus has a single point of contact, the loading nose, which applies the load to the sample midway between the support span of the

lower component. The radius of all contact points on the flexural testing apparatus is 5 mm. Prior to running the test, a small preload of ~ 18 N was applied to the sample. The complete list of experimental parameters used is outlined in Table 2 alongside the tensile test parameters. It should be noted, that ASTM standard D790 requires the support span be 16 ± 1 times longer than the depth and that the ends of the sample have an overhang of 10% of the support span extruding beyond the lower supports. The small samples can meet this requirement whilst the large samples maintain a span-to-depth ratio of approximately 4:1. The effects of this are discussed more in the results section.

The MTS software provides data for the applied force and the loading nose displacement. This must be converted into flexural stress and flexural strain according to Eqs. (1) and (2), respectively,

$$\sigma_f = \frac{3PL}{2bd^2} \quad (1)$$

$$\epsilon_f = \frac{6Dd}{L^2} \quad (2)$$

where P is the load, L is the span between the supports, b is the sample width, d is the sample depth, and D is the midspan deflection which is identical to the position of the loading nose. After the stress vs. strain curves are built, the maximum flexural stress and the flexural modulus of elasticity are found for each sample in an identical manner as outlined in the tensile test section.

2.3. Light output testing

The samples used for light output testing were taken from the ends of the mechanical testing samples after breaking since the material experiences little to no mechanical stress at the ends of the sample during the mechanical testing procedure. The samples were cut into a rectangular prism with nominal dimensions of $12 \times 12 \times 3$ mm. The samples were then incrementally polished on all sides with polishing pads up to a grit size of 2000P which has an average abrasive particulate size of $10.3 \mu\text{m}$. The samples were then visually inspected for fracturing, as fractures in these materials are highly visible due to Fresnel reflection at the fracture boundary. No fracturing was evident under visual inspection.

The 12×12 mm side of the sample was mounted to a Hamamatsu R2059 PMT using Visilox V-788 optical coupling compound. The maximum quantum efficiency of the R2059 PMT in the blue spectrum matches well with the peak emission of EJ200. The sample was then covered with seven layers of white Teflon tape and sealed using four layers of black electrical tape. The PMT was operated at a bias of -1550 V. The anode signal was split and sent to the trigger channel and standard channel of a CAEN DT5742b digitizer configured to acquire 1024 data samples per event at a sampling rate of 5 GS/s. A $1 \mu\text{Ci}$ Cs-137 source was placed 15 mm from the outer face of the scintillator sample. With the source present, the PMT was allowed to stabilize for 40 min on the first sample of each measurement day while same-day subsequent measurements allowed 10 min of stabilization time. The waveforms were utilized to calculate the integrated charge spectrum during post processing.

To calculate the integrated charge, the current was found via Ohm's Law and integrated. The signal voltage was determined by distributing the 1 V dynamic range across the 2^{12} ADC channels (0.244 mV/ADC channel) and the digitizer input impedance is 50Ω . The signal baseline was determined by averaging the first 10% of samples (102 samples) for each event and then the waveform was transformed via a standard baseline correction. The integration window was set to begin 15 ns before the signal peak and end 75 ns after the signal peak which is sufficient for the typical rise/and fall times of the measured pulses, which are approximately 3 ns and 20 ns respectively. The waveform was integrated using trapezoidal integration and the resulting integral value was placed into a histogram structure containing 800 bins ranging from 0–150 pC. The histogram structure was transformed from having bin edges to having a bin value on the charge axis which is the average of the bin edges. This allowed the data to be smoothed and differentiated

using a Savitsky–Golay filter [11]. The filter parameters for smoothing included using a window size of 31 bins with a second order filter. To differentiate the data, the same filter parameters were used on the smoothed data but with the additional filter parameter of 1st order derivative. The inflection point in the spectral neighborhood of the Compton edge was used as the location of the real Compton edge energy of 478 keV. This occurs at the minimum of the calculated derivative and the process is better demonstrated in Section 3.3.

Since the light output measurements occurred on four separate days, the EJ200 sample was measured at the beginning of each measurement day to calculate a daily correction factor to adjust for any environmental effects and or systematic effects in the measurement system. This factor was calculated as follows:

$$cf_n = \frac{CE_0}{CE_n} \quad (3)$$

where CE_0 is the Compton edge location on the charge axis for the very first EJ200 light output measurement and CE_n is the Compton edge location for the EJ200 light output measurement taken at the beginning of the n th measurement day. This correction factor was multiplied into the value of the Compton edge for all samples measured on the identical n th measurement day. It should be noted that the correction factor had values of 1.002, 1.002, and 1.012, which indicates that the systematic error introduced approximately 1–1.5% error to these measurements; the intent is that this error has been reduced by utilizing the correction factor. Regardless though, the error cannot be reduced below the 0.2% level due to the data binning structure. After the Compton edge is located on the integrated charge axis, the value is normalized to that of the PVT based EJ200. For reference, EJ200 has a light output of 10,000 photons per MeV [12].

3. Results and discussion

In order to have a meaningful picture of the mechanical testing data, the relevant values for two common structural plastics, acrylonitrile butadiene styrene (ABS) plastic and polylactic acid (PLA) based plastic are also provided. These values come from Matweb in the categories of “Overview of material for ABS, sheet” [13] and “Overview of material for PLA biopolymer” [14].

3.1. Tensile test results

The results of the tensile tests are shown in Figs. 2 and 3. There is good agreement within the bounds of statistical uncertainty across the two different sample types (type IV and type V) in the two cases where the same material was used: EJ200 and EJ200PS. This is due to the fact that the cross sectional area used to calculate the stress and the applied stressing force are parallel to each other. This makes calculating the stress, which is a pressure (force per unit area), a rather straightforward operation, even for the two different sample sizes. Aside from assessing that the materials across sample types can be directly compared, it is also apparent that while three of the materials are stronger than the average ABS plastic, none are stronger than the average PLA plastic. On the other hand, all the materials are stiffer (have a higher tensile modulus) than the average ABS plastic whilst four of the tested materials are stiffer than even the average PLA plastic. In general, this appears to indicate that plastic scintillators tend to be slightly more brittle than the common structural ABS and PLA plastics.

When identifying the effects of modifications to a particular plastic base (e.g., crosslinking EJ200PS) several things stand out. The first thing that stands out (and has been previously known) is that the polymer base matters; the PVT based EJ200 is not quite as strong or stiff as the PS-based counterpart. Additionally, it is apparent with these results that crosslinking as implemented has a larger effect on some base/fluor mixtures than others. For instance, a significant increase in the strength and stiffness of EJ299-33 can be observed in its crosslinked counterpart EJ299-33-XL, but this effect is not as dramatic when one compares

Table 2
Mechanical testing parameters.

Test material	Tensile test parameters					Flexural test parameters					
	Sample type	N samples	Measured or nominal dimensions	Crosshead rate (mm/min)	Sampling rate (Hz)	Sample type	N Samples	Measured or nominal dimensions	Support span (mm)	Crosshead rate (mm/min)	Sampling rate (Hz)
PD-02-55.02	V	5	Meas.	0.3	50	Sm.	5	Meas.	52	1.387	50
PD-02-55.02(Sn)	V	6	Meas.	0.3	50	Sm.	7	Meas.	52	1.387	50
EJ200	V	5	Meas.	0.3	50	Sm.	5	Meas.	52	1.387	50
EJ200-PS	V	5	Meas.	0.3	50	Sm.	5	Meas.	52	1.387	50
EJ200	IV	5	Nom.	1.5	100	Lg.	5	Nom.	100.3	0.256	100
EJ200-PS	IV	5	Nom.	1.5	100	Lg.	5	Nom.	100.3	0.256	100
EJ200-PSXL	IV	5	Nom.	1.5	100	Lg.	5	Nom.	100.3	0.256	100
EJ299-33	IV	5	Meas.	0.75	50	Lg.	4	Meas.	101	0.675	50
EJ299-33-XL	IV	5	Nom.	1.5	100	Lg.	5	Nom.	100.3	0.254	100
N555V	-	-	-	-	-	Lg.	4	Meas.	101	0.675	50

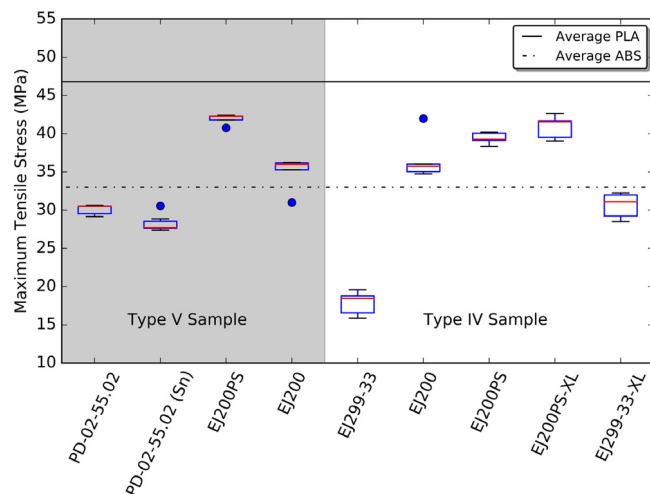


Fig. 2. Boxplot of the maximum tensile stress (MPa) of the tested materials shown alongside average PLA and ABS values.

the results from EJ200PS to EJ200PS-XL. This could be due perhaps to the particular choice in the crosslinking molecule for EJ200PS or due to an upper limit on the added strength which can be provided by crosslinking molecules in reference to the initial strength of the base. Lastly, it appears that by doping in organometallic complexes, at least as implemented in the 5% tin loaded sample, a very small or perhaps negligible decrease in strength and stiffness results.

3.2. Flexural test results

The results for the flexural tests are highlighted in Figs. 4 and 5. Unlike in the case of the tensile testing, the results generated from the large and small flexural samples of the same material do not agree. The stress calculation is not so straightforward since the force and resisting cross sectional area are perpendicular to each other. Because of this, Eqs. (1) and (2) from ASTM D790 are likely based on a set of assumptions which only make them valid in the regime where the span to depth ratio of the sample is approximately 16:1. This is where it is believed that the discrepancy originates between the results from the large and small flexural test specimens of the same material. Despite this fact, it is observed in the figures that the difference in the measured means of maximum flexural stress between the two baseline materials (EJ200 and EJ200PS) within the small and large size classes is statistically identical, having a value of 11 ± 6 MPa for the small samples and 9.1 ± 1.7 MPa for the large sample sizes. This may imply that the results from the large samples can easily be mapped to the same scale of comparison as the small samples by adding a baseline shift of 14 ± 4 MPa to their maximum flexural stress values.

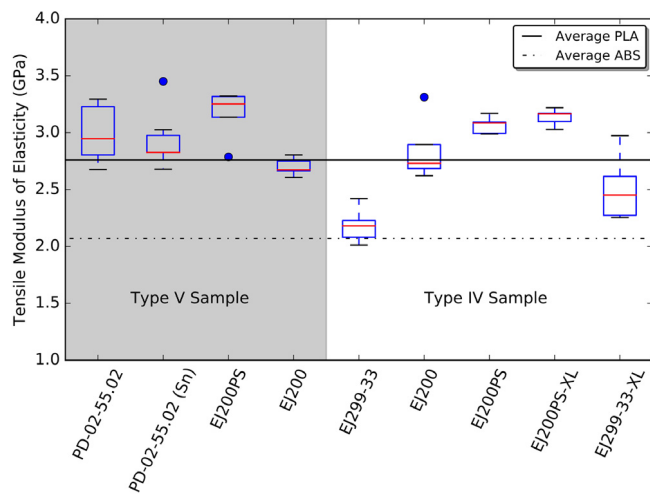


Fig. 3. Boxplot of the tensile modulus of elasticity (GPa) of the tested materials shown alongside average PLA and ABS values.

This type of direct mapping does not appear to be applicable in the case of the flexural modulus. Instead, a qualitative reasoning can be used by comparing other materials of the same size to the EJ200 and EJ200PS values within both size classes. For example, in Fig. 5 it is apparent that PD-02-55.02 has a somewhat smaller flexural modulus than EJ200 when comparing within the small sample class. This means, then, that within the large sample class it can be expected that PD-02-05.22 is also somewhat less than EJ200 which further implies that PD-02-05.22 is not as stiff as N555V, EJ200PS, and EJ200PS-XL.

Using the means of comparison given above, the flexural testing results, and the conclusions which can be drawn from them, are quite similar to the results and conclusions provided by the tensile tests. Perhaps the primary exception to this is that the flexural modulus of the tested materials does not appear to exceed the flexural modulus of PLA plastic to the same level as observed with the tensile modulus.

3.3. Light output testing

Fig. 6 illustrates how the Compton edge energy is determined from the integrated charge spectrum using the inflection point methodology. All numerical values are reported in Table 3 as being relative to EJ200. As indicated by Fig. 6 and Table 3, all light output values are relatively close to each other with the most collected charge coming from EJ200 and the least coming from N555V. Crosslinking has no noticeable effect on the light output of EJ200PS and only a minimal effect on EJ299-33. The addition of Sn to PD-02-05.22 appears to have a negligible effect on the light output.

Table 3
Test results.

Test material	Sample type	Tensile strength (MPa)	Tensile modulus of elasticity (GPa)	Sample type	Flexural strength (MPa)	Flexural modulus of elasticity (GPa)	Relative light output at 478 keV, \pm .01
PD-02-55.02	V	30.1 \pm 0.6	2.99 \pm 0.24	Sm.	68.9 \pm 0.9	2.64 \pm 0.07	0.82
PD-02-55.02(Sn)	V	28.3 \pm 1.1	2.94 \pm 0.25	Sm.	59.7 \pm 2.9	2.74 \pm 0.07	0.83
EJ200	V	34.9 \pm 2.0	2.70 \pm 0.07	Sm.	60 \pm 5	2.930 \pm 0.026	1.00
EJ200-PS	V	41.9 \pm 0.6	3.16 \pm 0.20	Sm.	72 \pm 4	3.57 \pm 0.04	0.91
EJ200	IV	36.7 \pm 2.7	2.85 \pm 0.27	Lg.	48.6 \pm 1.0	2.017 \pm 0.026	1.00
EJ200-PS	IV	39.4 \pm 0.7	3.07 \pm 0.07	Lg.	57.7 \pm 1.4	2.474 \pm 0.008	0.91
EJ200-PSXL	IV	40.9 \pm 1.4	3.14 \pm 0.07	Lg.	64.0 \pm 2.8	2.470 \pm 0.022	0.91
EJ299-33	IV	17.9 \pm 1.4	2.18 \pm 0.14	Lg.	27.8 \pm 0.5	1.545 \pm 0.023	0.87
EJ299-33-XL	IV	30.6 \pm 1.5	2.51 \pm 0.27	Lg.	73.0 \pm 0.9	1.83 \pm 0.04	0.83
N555V	-	-	-	Lg.	73 \pm 8	2.06 \pm 0.05	0.77

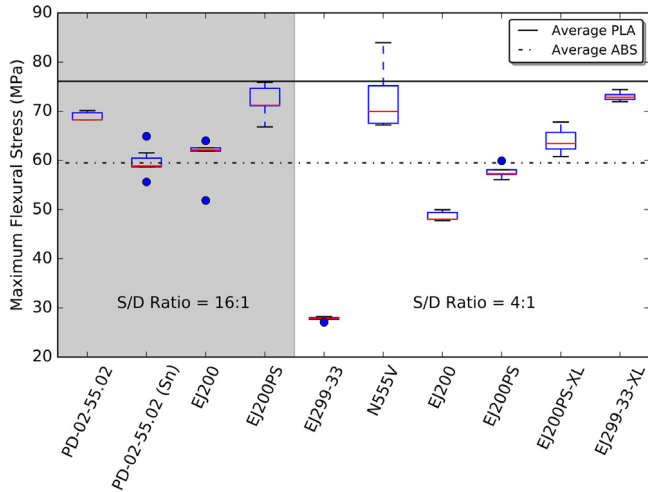


Fig. 4. Boxplot of the maximum flexural stress (MPa) of the tested materials shown alongside average PLA and ABS values.

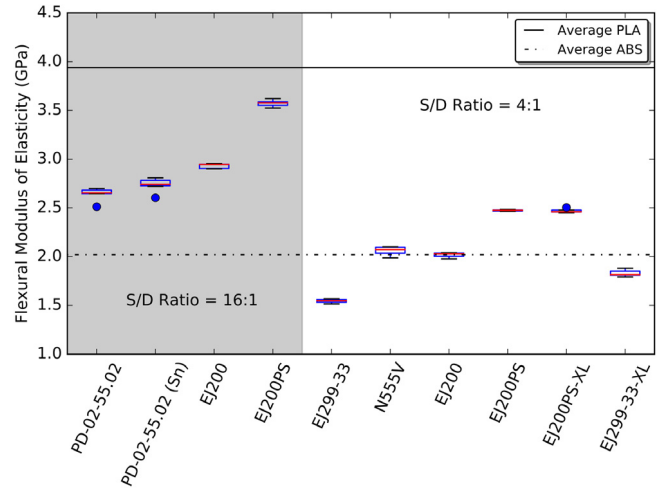


Fig. 5. Boxplot of the flexural modulus of elasticity (GPa) of the tested materials shown alongside average PLA and ABS values.

4. Conclusion

We have made measurements on a variety of plastic scintillating materials to gather data that may help one (1) determine whether these scintillating materials are suitable as structural materials for particular applications and (2) better understand the expected effects of chemical modifications, such as crosslinking or doping organometallic complexes into the polymer matrix, on the mechanical and radiation detection properties. Crosslinking the matrix can significantly improve

the mechanical strength and this has been demonstrated to have a most significant effect when the polymer has been quite loaded with fluors, as in the case of EJ299-33, to the point that it becomes soft. However, the effect of crosslinking on the mechanical properties of an organic scintillator is not always observed to be so significant. Either by properties of the base material, crosslink selection, or combination of the two, a gain in mechanical strength is not always observed, as in the case of crosslinking EJ200PS. The effect of crosslinking on light output appears to be minimal with only a 5% loss observed by crosslinking

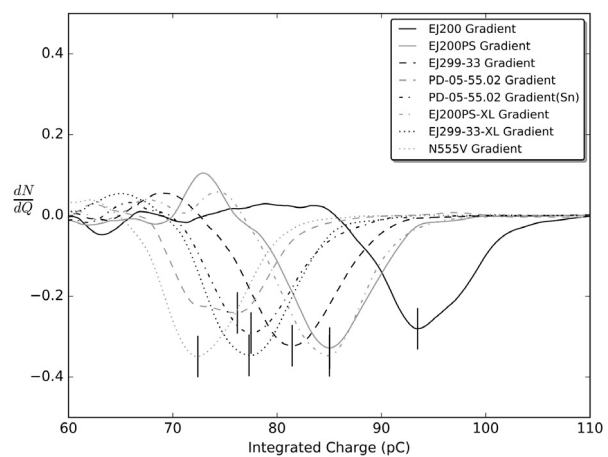
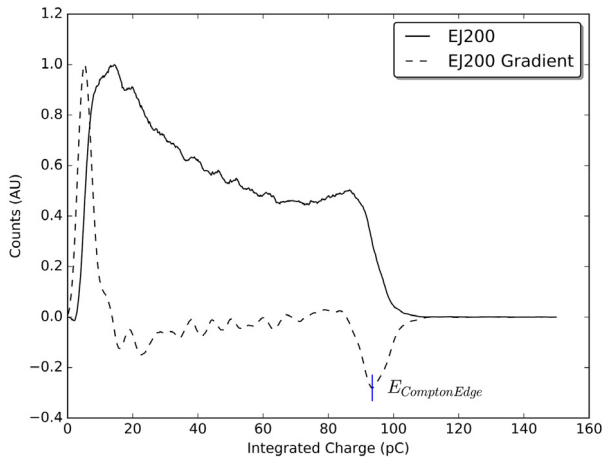


Fig. 6. Demonstration of locating the Compton edge on the Cs-137 spectrum using the inflection point found by the derivative (left). Location of the Cs-137 inflection points for all investigated materials (right).

EJ299-33 and no loss observed by crosslinking EJ299PS. Doping Sn based organometallic complexes into PD-02-55.02 did cause a decrease in the mechanical strength of this material, but it also appears to have slightly increased the light output.

These findings further indicate that the mechanical strength of most of the tested organic scintillators is comparable to and in some cases greater than that of ABS plastic, though not necessarily as strong as the more robust PLA plastic. Further still, it has been shown that chemical methods can effectively be utilized to enhance mechanical properties of the material without having a significant impact on the light output of the scintillator, which is important for radiation detection and identification purposes.

Acknowledgments

This material is based on work supported in part by the Defense Threat Reduction Agency, United States under grant number HDTRA 1-18-1-005, in part by the Department of Energy National Nuclear Security Administration, United States through the Nuclear Science and Security Consortium under Award Number DE-NA-0003180, and in part by BAE Systems, United States Contract No. W911NF-08-2-0004.

References

- [1] Y. Chen, C. Liu, Y. Jin, T.J. Hajagos, D. Kishpaugh, Q. Zhuang, et al., Ytterbium fluoride loaded plastic scintillators for γ -ray spectroscopy, in: *SPIE Optical Engineering + Applications*, 2016, p. 12.
- [2] N.J. Cherepy, R.D. Sanner, P.R. Beck, E.L. Swanberg, T.M. Tillotson, S.A. Payne, et al., Bismuth- and lithium-loaded plastic scintillators for gamma and neutron detection, *Nucl. Instrum. Methods Phys. Res. A* 778 (2015) 126–132.
- [3] P.L. Feng, W. Mengesha, M.R. Anstey, J.G. Cordaro, Distance dependent quenching and gamma-ray spectroscopy in tin-loaded polystyrene scintillators, *IEEE Trans. Nucl. Sci.* 63 (2016) 407–415.
- [4] N. Zaitseva, A. Glenn, L. Carman, H. Paul Martinez, R. Hatarik, H. Klapper, et al., Scintillation properties of solution-grown trans-stilbene single crystals, *Nucl. Instrum. Methods Phys. Res. A* 789 (2015) 8–15.
- [5] N. Zaitseva, B.L. Rupert, I. Pawełczak, A. Glenn, H.P. Martinez, L. Carman, et al., Plastic scintillators with efficient neutron/gamma pulse shape discrimination, *Nucl. Instrum. Methods Phys. Res. A* 668 (2012) 88–93.
- [6] P.N. Zhmurin, V.N. Lebedev, V.D. Titskaya, A.F. Adadurov, D.A. Elyseev, V.N. Pereymak, Polystyrene-based scintillator with pulse-shape discrimination capability, *Nucl. Instrum. Methods Phys. Res. A* 761 (2014) 92–98.
- [7] T.J. Hajagos, D. Kishpaugh, Q. Pei, Pulse shape discrimination properties of plastic scintillators incorporating a rationally designed highly soluble and polymerizable derivative of 9,10-diphenylanthracene, *Nucl. Instrum. Methods Phys. Res. A* 825 (2016) 40–50.
- [8] C. Burt, D. Ramsden, The development of large-area plastic gamma-ray spectrometers, in: 2008 IEEE Nuclear Science Symposium Conference Record, 2008, pp. 1186–1190.
- [9] ASTM International, Standard Test Method for Tensile Properties of Plastics, D638, ed. West Conshohocken, PA, 2014.
- [10] ASTM International, Standard Test Methods for Flexural Properties of Unreinforced and Reinforced Plastics and Electrical Insulating Materials, D790, ed. West Conshohocken, PA, 2015.
- [11] A. Savitsky, M.J.E. Golay, Smoothing and differentiation of data by simplified least squares procedures, *Anal. Chem.* 36 (1964) 1627–1639.
- [12] Eljen Technology. (2016, July 27, 2018). GENERAL PURPOSE EJ-200, EJ-204, EJ-208, EJ-212. Available: <https://eljentechnology.com/products/plastic-scintillators/ej-200-ej-204-ej-208-ej-212>.
- [13] Matweb. (May 18, 2018). Overview of materials for Acrylonitrile Butadiene Styrene (ABS), Sheet. Available: <http://www.matweb.com/search/DataSheet.aspx?MatGUID=c8bc69525dd04bd9bca54c475f6b38c3&ckck=1>.
- [14] Matweb. (May 18, 2018). Overview of materials for Polylactic Acid (PLA) Biopolymer. Available: <http://www.matweb.com/search/DataSheet.aspx?MatGUID=ab96a4c0655c4018a8785ac4031b9278>.